PROCEEDINGS, Twenty-Fourth Workshop on Geothermal Reservoir Engineering
Stanford University, Stanford, California, January 25-27, 1999
SGP-TR-162

FRACTURE DISPERSION EFFECTS IN TRACER ANALYSIS

R. Schroeder [1], D. Swenson [2], N. Shinohara [3], T. Okabe [3], N. Shinohara[3]

[1] Berkeley Group Inc.
245 Gravatt Drive
Berkeley, California, USA, 94705
rcsch@slip.net

[2] Kansas State University
Manhattan, Kansas, USA, 66506
swenson@ksu.edu

[3] Geothermal Energy R. & D.
Kyodo Bldg.
Chuo-Ku, Tokyo 103, Japan
rd.dep@gerd.co.jp

ABSTRACT

Hydraulic dispersion in porous media and in fracture networks results in the spreading of the time-dependent tracer signal. In geothermal reservoirs the wellbore often intersects fractures that are separated by tens or even hundreds of meters. The mixing in the wellbore at those separated fractures is also a source of dispersion, since tracer signals sampled at the wellhead are a mixture of the individual tracer signals arriving from all fractures intersected by the production wellbore.

The dispersion in reservoir fractures is most heavily dependent upon mixing and spreading at fracture joints. In this paper we discuss the relevant reservoir and wellbore dispersion phenomena and compare calculated tracer signals with measured tracer data for a case of low flow rates and widely spaced fractures.

INTRODUCTION

Dispersion is a phenomenon in which a specified concentration of a tracer is diluted by: 1) mixing with a second concentration during hydrodynamic flow and 2) by spreading spatially through a network of connected pathways.

Bear describes two phenomena associated with dispersion: molecular diffusion, and convection (Bear, 1975). Molecular diffusion typically occurs at much slower rates than convection in fractured geothermal reservoirs and is not considered in this report.

Dispersion in fracture networks is similar to the dispersion seen in Figure 1. When time delays between fractures and mixing take place in a wellbore that intersects widely separated fractures, another form of dispersion appears. The importance of wellbore dispersion is that if it is not taken into account the reservoir dispersion parameters obtained from tracer tests, such as the macroscopic dispersion-coefficient, can be seriously in error.

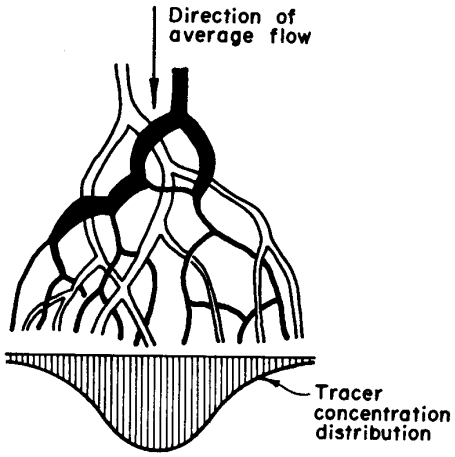

Figure 1. Dispersion in porous media.

Tracer tests have been carried out at the Hijiori circulation test site, and some data from those tests are analyzed using the fractured-reservoir simulator, GEOCRACK (Swenson, 1997), and the wellbore simulator, WELF98. GEOCRACK is a two-dimensional code, and the limitations this imposes on the tracer analysis are discussed below.

In previous reports we have documented the Hijiori reservoir geology, fracture characteristics, and the test data, so that information will not be repeated again (Schroeder and Swenson, 1998). It is useful to remember that the Hijiori reservoir lies on the edge of a caldera and that the wells intersect steeply dipping ring fractures that strike in an east-west direction. The wells intersect the upper fracture at about 1780 m depth and the lower fracture at about 2165 m. Test data indicates that other fractures intersect the wellbore, and joints connect the two major fractures.

WELLBORE DISPERSION

There is more than one source of dispersion in the injection and production wellbores. One source of dispersion is the mixing that occurs due to viscous hydrodynamic flow in the injection and production wellbores. A second is mixing that occurs in the production wellbore as flow from the reservoir enters the wellbore. A third is due to time delays between fractures. In this report we discuss only dispersion associated with flow entering the wellbore from widely separated fractures.

Typically, tracers are injected into the injection well at a constant rate for a specified length of time as shown in Figure 2. This is the type of test that will be discussed in this report.

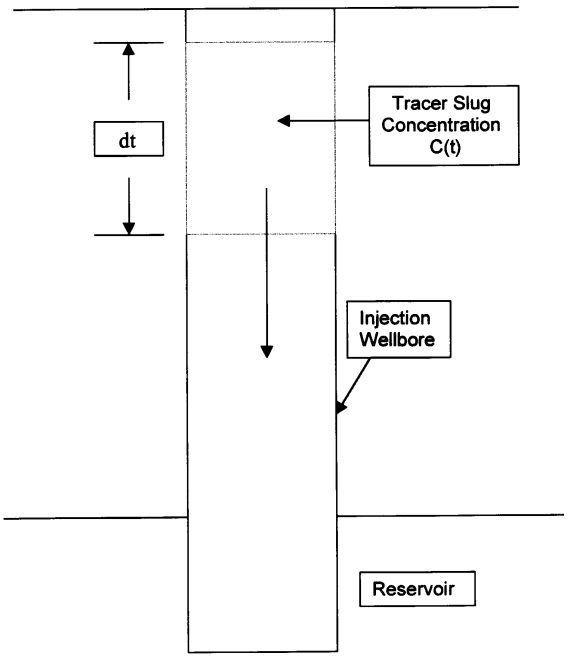

Figure 2. Tracer injection over a specified time period

Injection Well

Injection into geothermal wells can be done with a wellhead pressure, or in many cases, on a vacuum. The latter means that the reservoir can accommodate the injection flow rate, and the wellbore liquid surface is below the wellhead. In that case the fluid above the liquid column is dispersed mist or steam. For simplicity we do not consider that case in this report.

There is no fracture-separation mixing effect in injection wells, but there can be significant time delays for the tracer injection into separated fractures.

For the case of two fractures, as shown in the example of Figure 3, the time between injection into fracture 1 and fracture 2 is given by

$$d(t) = \frac{3\Delta z_f \; r \; A}{2q}$$

where the mass flow rate is q, and A is the wellbore cross-sectional area.

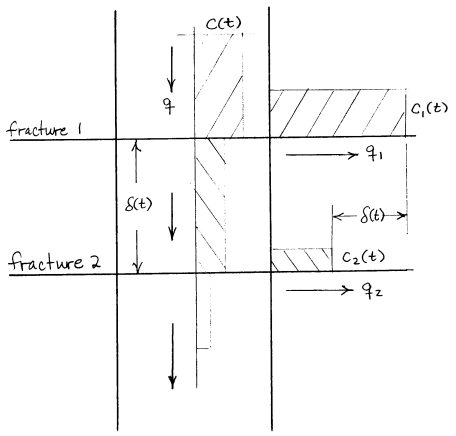

Figure 3. Injection into separated fractures.

The time from the second to a third fracture will be twice as long, since the flow rate is q/3. Typical values for pipe diameter and injected fluid density give the approximate time in seconds for fluid to move between fracture 1 and fracture 2.

$$t_{12} \approx 300 \frac{\Delta z_f}{q}$$

Typical geothermal fracture spacing is from 10 to 100 m, and typical geothermal injection flow rates are from 10 to 100 kg/s. Thus the smallest time intervals from fracture 1 to fracture 2 and fracture 1 to fracture 3 range from 0.5 to 1.5 minutes, and the maximum time intervals range from 50 to 150 minutes, respectively.

For large flow rates and small fracture spacing the delay of the injection into the second and third fractures is obviously negligible. However, the time delay between the upper-most and deepest fracture for large separations and/or low flow rates can be very significant. The effect of the injection time-delay between the shallow and deeper fractures is to

delay the arrival time of the flow from deeper fractures at the production well. Thus, for connected fracture networks the injection time-delay produces the same apparent effect on the sampled tracer signal as reservoir dispersion.

Production Well

The arrival time of the reservoir tracer signal at each fracture intercepted by the production wellbore can be different due to the different reservoir flow paths for each of the wellbore fractures. As the fluid moves up the production wellbore from the deepest fracture to the fracture with the shallowest depth, mixing of fluids in the wellbore occurs at each of the fractures.

Figure 4 shows the effects of mixing at each fracture as the flow proceeds up the wellbore. It is clear from Figure 4 that the contribution from each subsequent fracture must be "folded" together with the flow (tracer signal) coming up the wellbore from below.

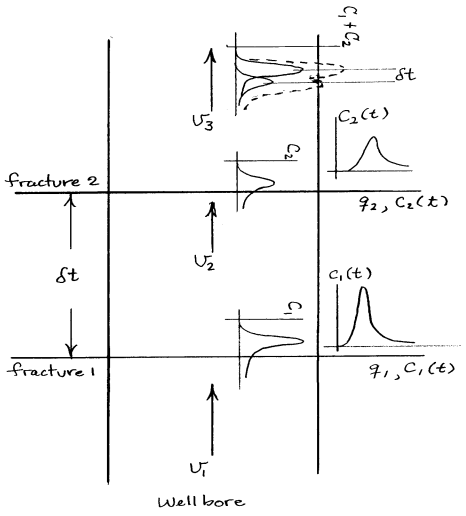

Figure 4. A figurative description of fracture separation.

At each fracture the conservation equations give the mixture concentration

$$C_2(t) = \frac{q_1 C_1(t) + q_f C_f(t)}{q_1 + q_f}$$

where C is the specific tracer concentration, and the subscript 1 refers to the flow below the fracture and 2 is for above the fracture.

The mixing at each wellbore fracture results in a final wellhead tracer signal that can appear to have significant reservoir dispersion, but has actually been altered by the wellbore dispersion due to the fracture spacing.

1991 HIJIORI TRACER DATA

Detailed descriptions of the Hijiori circulation system (wells and reservoir) have been given previously and need not be repeated here (NEDO 1996, 1997). In addition to several well tests, several tracer tests have been performed at Hijiori. We will use data from tracer tests carried out in 1991.

In 1991 the well SKG-2 was used for injection and wells HDR-1, 2, and 3 were used as producers during a series of tracer tests. Table 1 shows the tracers used during those tests.

The detailed tracer methodology used in these tests is not the emphasis of this report, and descriptions of those tests can be found elsewhere. Our effort is applied to model the effects of reservoir and wellbore dispersion.

Test	Date and time of injection into SKG-2	Tracer Type (kg)
1	8/19/91, 0:00 (day 17)	KI(5.0), KBr(4,9)
2	8/30/91, 9:00 (day 28)	KI(6.0), Mo(5.0)
3	9/9/91, 16:00 (day 38)	KBr(4.1), W(5.1)
4	9/19/91, 16:00 (day 48)	KI(3.0), Mo(3.0)
5	10/2/91, 16:00 (day 61)	KBr(5.0), W(5.0), Fl(25g)
6	10/31/91, 16:00 (day 91)	KI(5.0), Mo(3.0), Fl(25g)

Table 1. Six tracer tests were done using alkaline-halide, heavy metal, and fluorescein tracers.

During the 1991 Hijiori tracer tests the wells HDR-2 and HDR-3 were used as the production wells. Figure 5 shows the measured tracer signals sampled at those production wells. For simplicity we will only discuss the data and analyses from the first tracer test shown in Table 1.

WELF98 CALCULATIONS

Wellbore calculations using WELF98 have been made to determine the flow rates and temperatures in each of the fractures intercepted by the production wells. This has previously been documented (Schroeder and Swenson, 1998) and will not be

repeated here in detail. We will however, give some of the results that are important to the tracer analysis.

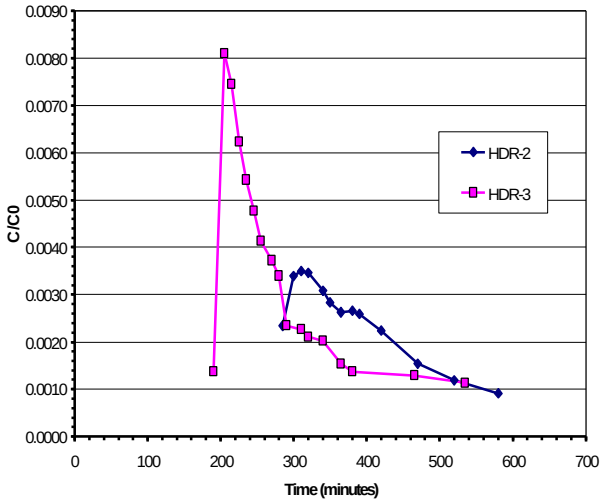

Figure 5. The 1991 tracer data for the first test.

HDR-2a Flow Rates

The WELF98 calculated data relevant to the tracer analysis is given in Tables 2 and 3. The temperatures in Table 2 were calculated by WELF98 from measured wellbore data. These tables summarize calculations for the dates when production was from HDR-2, and HDR-3.

Depth (m)	Pressure (Mpa)	Temp (C)	Flowrate (kg/s)
1565	13.077	223.4	0.53
1595	13.302	218.6	0.475
1650	13.755	214.8	0.593
1670	13.884	211.2	0.593
1755	14.568	162.1	0.593
1765	14.632	197.3	1.009
1781	14.726	215.5	0.593
1808	14.911	236.1	0.2375
1830	15.063	246.2	0.11875
1900	15.6	260	0.02

Table 2: HDR-2 WELF98 results for 8/13/91

HDR-3 Flow Rates.

Similar calculated data for HDR-3 at the times when all wells are producing are given in Table 3.

Depth (m)	Pressure (Mpa)	Temp (C)	Flowrate (kg/s)
1550	14.156	200.1	0.663
1651	15.004	216.1	0.9945
1754	15.857	167.8	2.65
1759	15.857	209.1	1.328
1861	16.65	245.9	0.9945
1900	16.95	257.5	0.02

Table 3. HDR-3 WELF98 data for 8/14/91

Transit Times

Tables 4 and 5 give the transit times for the two production wells calculated by WELF98. The transit time for the injection well, SKG-2, was calculated to be 41 minutes to the fracture at the depth of 1780 m. The injection well, SKG-2, intercepts only one fracture, and is cased above that fracture.

Marker Release depth (m)	Velocity (m/s)	Time to WH (min)
1831	<.01	457
1808	<.01	304
1779	0.03	256
1765	0.05	247
1755	0.07	244
1680	0.08	225
1650	0.1	219
1595	0.11	210
1565	0.13	205

Table 4: HDR-2a transit times

Marker Release depth (m)	Velocity (m/s)	Time to WH (min)
1861	<.01	344
1759	0.06	170
1754	0.13	168
1651	0.17	155
1550	0.18	144

Table 5. HDR-3 transit times

GEOCRACK CALCULATIONS

A GEOCRACK model consists of two-dimensional rock blocks with nonlinear contact and discrete fluid paths between the blocks. Heat transfer occurs by

conduction in the rock blocks and transport in the fluid. The user interactively defines the finite element mesh, the material properties, boundary conditions, and solution controls

The GEOCRACK model of the Hijiori circulation system used for this analysis has previously been described in Schroeder and Swenson, 1998, and only a summary description will be repeated. Figure 6 shows the rock blocks (rectangles), fracture/flow paths (blue paths), and well locations (circles and squares) in the model. In 1991, injection was at the upper fracture in SKG-2.

The GEOCRACK model of Hijiori represents a vertical section of the reservoir, extending from a depth of 1475 to 2475 m. The horizontal extent is 1000 m, with the wells approximately centered within the model. The vertical section used for the model was chosen to bound the known volume of the reservoir. A uniform depth of 50 m was used for the entire model. This is an estimate of the participating depth of flow on the steeply dipping fractures known to exist at Hijiori. It was selected to be on the same order as the spacing between the wells.

The horizontal spacing of the fractures is 75 m with a vertical spacing of 100 m (these values are for the region in the center of the model). The spacing used for these fractures was based on the approximate number of known fractures that intersect the wells. Also, the pattern of the fractures was chosen to enhance the vertical connection between the upper and lower fractures, since there is a known connection between them.

Material Properties

Since GEOCRACK solves the coupled fluid/thermal/structure problem, all associated properties must be specified. The in-situ stresses at Hijiori are 43.2 MPa horizontal, 54.0 MPa overburden, and 32.4 MPa minimum horizontal. The hydrostatic pressure at a depth of 2000 m is about 18.5 MPa. In the model, all other pressures were adjusted to the same depth, so that the relative values would be correct.

Rock and Water Properties

Standard properties for granite and water were used in the analysis. The water viscosity was specified as a function of pressure and temperature.

$$a = 0.25\left[1.0 - \left(\frac{s_{eff}}{75}\right)^{0.33}\right]$$

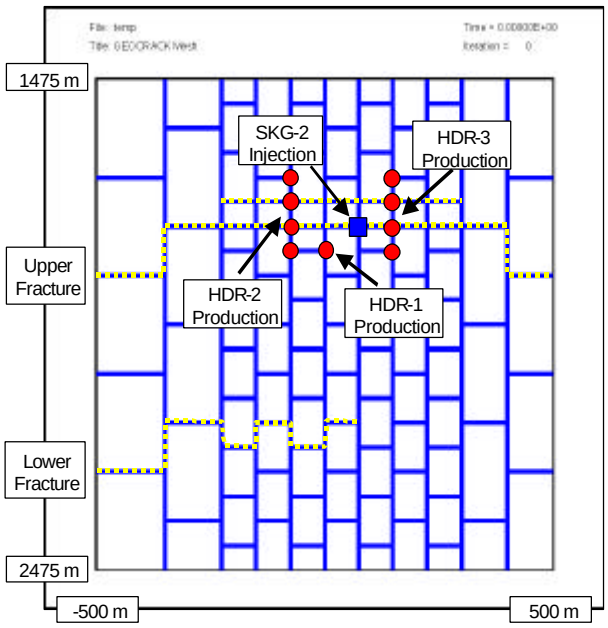

Figure 6: GEOCRACK model representing a vertical section of the Hijiori reservoir

This gives a nonlinear stiffness between opening and effective stress on the fracture. For example, at an effective stress of 35.5 MPa (54 MPa in-situ – 18.5 MPa hydrostatic), the fracture opening is 0.05468 mm. The same contact behavior was used for all fractures in the model.

Fracture	Initial Opening (mm)
Horizontal	0.075
Vertical	0.125
Horiz. Upper and Lower	0.200
Vert. Upper and Lower	0.250

Table 6: Initial fluid openings

Fluid Flow

In GEOCRACK, the problem is defined in an initial equilibrium state. The conductivity of the joint elements is calculated using the cubic law, $k_p = \frac{a^3}{12mf}$, where a is the joint opening, m is the dynamic viscosity, and f is an adjustment factor (assumed 1.5 in all calculations). The user specifies the initial opening at the equilibrium state, and then

any displacements are added to that value when calculating the conductivity, $a = a_0 + a_{displacement}$. If we strictly use the Gangi model the initial opening would be 0.055 mm at an effective stress of 35.5 MPa, however, for the flows to match the data and because of the known increased fracture conductivity at the upper and lower fractures, the values of the initial openings were specified as shown in Table 6.

Wellbore and Far-Field Boundary Conditions

In the Hijiori reservoir, the upper and lower fractures are conceived to be high conductivity fractures. The wellbores intersect this fracture. When water is injected into HDR-1, some of the water is recovered in HDR-2a and HDR-3, but some water flows past the production wells and into the far-field A two-dimensional model of a vertical section of the reservoir cannot accurately represent both the flow into the producing wells and flow past the wells.

To improve our representation of this flow condition, the concept of conductivity from the fractures to the wellbores and far-field was introduced. The user specifies a pressure in the wellbore (or far-field) and a corresponding conductivity from the fracture to the wellbore (or far-field). The flow into the wellbore is then calculated using this conductivity and the pressure difference between the wellbore and fracture, or,

$$Q = K_{well}\left(P_{fracture} - P_{well}\right)$$

This approach makes it possible to model the high conductivity upper and lower fractures and also to represent the partial flow of the water into the wellbores.

Pressures and Flows Used in Analyses

The analysis represents the Hijiori reservoir during 1991 testing. (Schroeder and Swenson, 1998) shows the conductivities and wellbore pressures used for the analyses. The wellbore pressures were based on WELF98 calculations. The conductivities were then selected to match the observed flow distributions. The conductivities show that the connections between the upper fracture and HDR-2a and HDR-3 are very good.

Tracer Model

GEOCRACK allows the user to specify a tracer boundary condition. After a converged solution is obtained, the flow rates are then used to calculate tracer concentrations. The tracer calculation is performed using a particle-tracking scheme. The advantage of this scheme is that it does not introduce numerical dispersion.

The user specifies the time during the analysis at which tracer is to be released at the injection point. At the specified time, a fixed number of particles (presently 100,000) are introduced to the model. Using the current fluid flow solution, each particle is traced as it flows through the model. At each flow junction, the path of the particle is determined randomly based on the proportion of flows at that junction.

Of course, flow in real fractures is much more complex than can be represented using only an average fluid velocity. Even if parallel fracture theory were exact, there would be a parabolic velocity distribution across a joint opening, so some fluid would move rapidly and some much slower. GEOCRACK allows the user to explore these effects. In addition, GEOCRACK allows the user to specify thermally reactive tracers and adsorbing tracers.

Two approaches are available for dispersion. The simplest assigns each particle a random thickness position in the parabolic velocity field. This velocity is used to move the particle. If the user wishes, the particle thickness position can remain constant or it can be randomly reassigned each time a fracture joint is reached. Such a model gives maximum dispersion.

Alternately, dispersion can be modeled by Taylor diffusion, which is a based upon a parabolic fluid velocity profile (Taylor, 1953). The dispersion component of particle movement is: $x_d = Z\sqrt{2D_L\Delta t}$ where Z is a normal distribution with a mean of zero and a variance of one, D_L is the coefficient of longitudinal diffusion, and Δt is the time step (Reimus 1995). For flow between parallel plates $D_L = D_b + v^2a^2 / 210D_b$, where D_b is the Brownian diffusivity, v is the average velocity, and a is the joint aperture (Kessler and Hunt, 1994). In addition, tracer particles may be influenced by adsorption and thermal degradation.

Since GEOCRACK couples the deformations due to hydraulic pressure and thermal strain with the state of stress, fluid volume and flow distribution change as the reservoir cools. Therefore, the residence time distribution and dispersion of a completely non-reactive tracer also change during heat mining. However, using the non reactive tracer as a standard for comparison, changes in the degrading and adsorbing tracers qualify and quantify changes in the surface areas and temperature characteristics of active flow paths.

The use of the GEOCRACK tracer models and comparisons with experimental data is described in

DuTeaux and Callahan, 1996, and in DuTeaux, Hardeman, and Swenson, 1996.

Limitations of Two-dimensional Modeling

Dispersion in porous media (fracture networks) is in general a tensor quantity (Scheidegger 1960, Bear 1975) and is inherently three-dimensional. For linear coordinates oriented along flow paths, dispersion can be modeled in terms of the transverse, horizontal, and longitudinal dispersion. Since GEOCRACK is 2D, and the Hijiori model is a vertical slice of the reservoir, the calculated dispersion does not include the horizontal component.

Also, at Hijiori the wells are inclined relative to the fractures and the current model does not include that feature. Inclination of the fractures and wellbores would increase the mixing at fracture joints. The result of the simplifying model assumptions is to underestimate the effect of dispersion for the conditions that were present during the Hijiori tracer tests.

RESULTS OF CALCULATIONS

Figure 7 shows the detailed flow of fluid in the GEOCRACK grid.

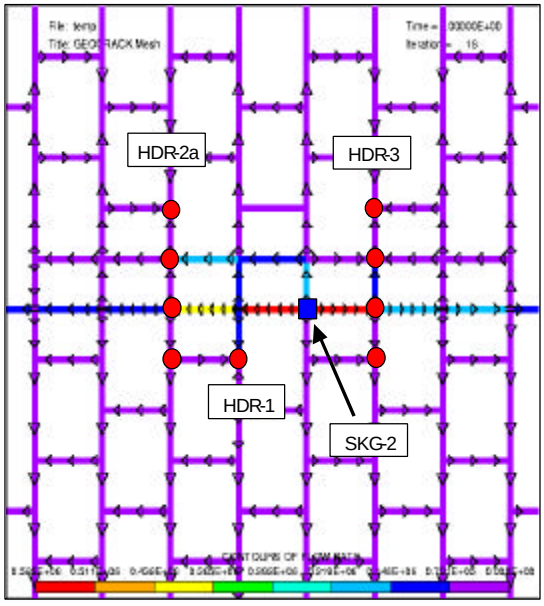

Figure 7. Detail of the flow in the fractures (min=0 kg/day, max=0.58E6 kg/day)

The measured wellbore data shows 8 to 10 fractures that have hydraulically paths between the wells. The model in Figure 7 has combined some of the fractures that are relatively closely spaced. This has the effect of underestimating the reservoir dispersion.

Reservoir Tracer Calculation Results

The reservoir tracer model has quadratic flow distribution in the fractures, with mixing at the joints. Figure 8 shows a plot of downhole tracer responses for each HDR-2 fracture in the model. The primary upper fracture flow path (1775 m) shows the fastest response. The calculated initial arrival in the main fracture time across the reservoir in HDR-2 is about 5 minutes.

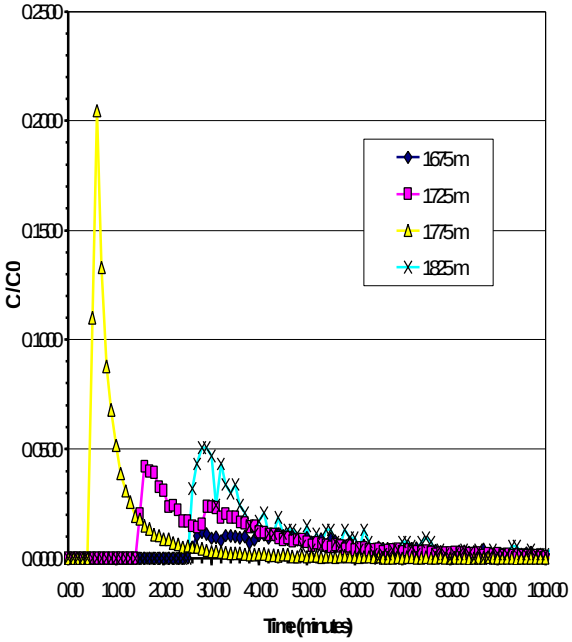

Figure 8: HDR-2a tracer for all producing fractures (time measures downhole transient, t=0 is time of SKG-2 injection at depth of 1775 m) with the WB mixture curve.

In 1991 at the upper fracture, the connection between SKG-2 and HDR-3 was even stronger than the connection between SKG-2 and HDR-2. The calculated fracture responses and mixture response are shown in Figure 9 for HDR-3.

Comparison with Measured Data

As previously discussed, the tracer measurements are made at the wellhead. Therefore, the fracture dispersion must be taken into account. The concentrations from each fracture were mixed according to the discussion given above, and the wellhead tracer response was calculated by GEOCRACK using the calculated results in Figures 8

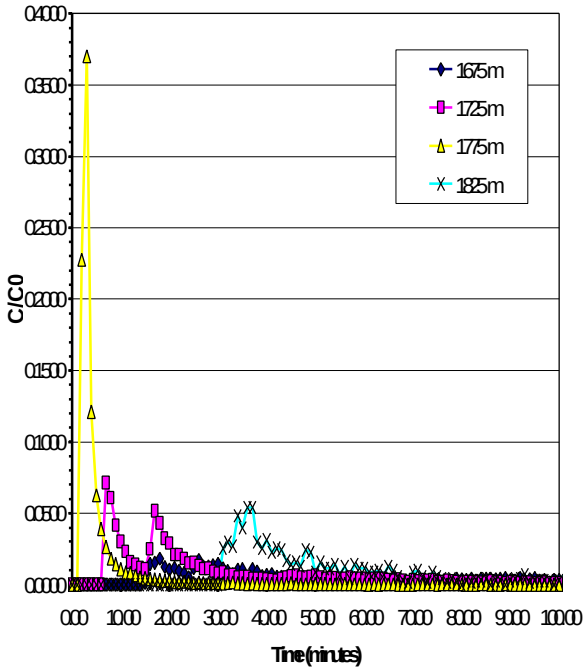

Figure 9: HDR-3 tracer for all producing fractures (time measures downhole transient, t=0 is time of SKG-2 injection at depth of 1775 m) with the WB mixture curve

and 9, and the transit times calculated by WELF98 given in Tables 4 and 5.

These comparison of the calculations and measurements is presented in Figure 10. These graphs have been normalized by the maximum concentration to allow comparison.

The calculated tracer response in Figure 10 shows much less dispersion than the measured responses from Figures 8 and 9, although the calculated arrival times show good agreement with the measured data. For example

- The calculated first arrival times at the wellhead match the observed data. This supports the conclusion that the fastest transit times across the reservoir are approximately 5 minutes, indicating some very direct connections between SKG-2 and HDR-2 and HDR-3 at the upper fracture.

SUMMARY

Wellbore dispersion effects arise from viscous hydrodynamic phenomena and widely spaced fractures. Wellbore dispersion appears in both the injection and production wells. The injection well dispersion is caused by delayed injection into widely spaced fractures as the injected pulse of tracer flows down the well. Production well dispersion is caused by both the delays between widely spaced fractures and by the mixing of the (in general) different time-dependent concentrations entering the wellbore from each fracture.

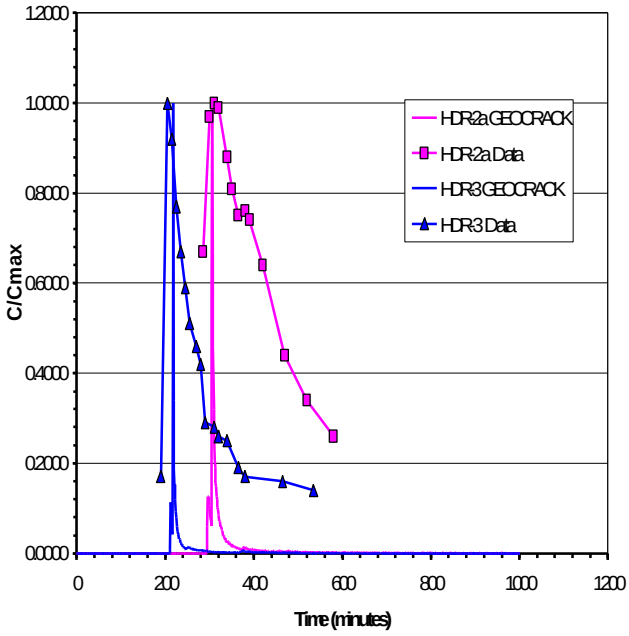

Figure 10. Predicted wellhead tracer response plots compared with measured data.

The wellbore simulator, WELF98, and the reservoir fracture simulator, GEOCRACK, incorporate models to take into account the effects of wellbore dispersion. Examples using data from the Hijiori, Japan experimental Geothermal Fracture Circulation site showed that t he GEOCRACK analysis predicts a faster decline of tracer (less dispersion) than observed in the data. This is at least partially due to the 2D model approximation to the real 3D problem, as discussed above. Other factors playing major roles in the poor comparison include:

- The importance of adsorption of tracer in the fracture network is not known and has not been quantified
- The amount of hydrodynamic dispersion in the injection and production wellbore has not been quantified
- GEOCRACK is a 2D model and cannot simulate all of the tracer dispersion in the fracture network. A 3D version will be applied in the future to simulate those effects

REFERENCES

Bear, Jacob, "Dynamics of Fluids in Porous Media", American Elsevier, 1975

DuTeaux, R., and Callahan, T. J., "Comparing Reactive and Non-Reactive Tracers to Measure Changes in Liquid Dominated, Fractured Geothermal Reservoirs," Proceedings of the Geothermal Resource Council Annual Meeting, 1996.

DuTeaux, R., Hardeman, B., and Swenson, D., "Modeling the Use of Reactive Tracers to Predict Changes in Surface Area and Thermal Breakthrough in HDR Reservoirs,"

Freeze, R. A., and J. A. Cherry, *Groundwater*, Prentice-Hall, Inc., 1979

GERD (Geothermal Energy Technology Department), "FY 1995 Summary of Hot Dry Rock Geothermal Power Project in Japan," New Energy and Industrial Technology Development Organization, Tokyo, Japan, September 1996.

Kessler, J. H., and J. R. Hunt, "Dissolved and colloidal transport in a partially clogged fracture", Water Resources Research, Vol. 30, No. 4, pp. 1195-1206, April 1994.

Levenspiel, Octave, *Chemical Reaction Engineering*, 2nd ed., John Wiley and Sons, Inc. 1972.

NEDO, "FY 1995 Summary of Hot Dry Rock Geothermal Power Project in Japan," New Energy and Industrial Technology Development Organization, Tokyo, Japan, September 1996.

NEDO, "FY 1996 Summary of Hot Dry Rock Geothermal Power Project in Japan," New Energy and Industrial Technology Development Organization, Tokyo, Japan, November 1997.

Scheidegger, A., The Physics of Flow Through Porous Media", Toronto Press, 1960.

Schroeder, R. and Swenson, Daniel, "Repeat of 1991-1996 Hijiori Reservoir Analysis," report prepared for GERD, July 1998.

Swenson, Daniel, "User's Manual for GEOCRACK: A Coupled Fluid Flow/Heat Transfer/Rock Deformation Program for Analysis of Fluid Flow in Jointed Rock," Manual Release 3.11b, Kansas State University, Manhattan, KS, 66506, March 1997.

Taylor, G., "Dispersion of Soluble Matter in Solvent Flowing Slowly Through a Tube", Proc. Roy. Soc., A, No. 1137, 1953.

ACKNOWLEDGEMENTS

We thank Geothermal Energy Research and Development Company, and NEDO for supporting this work.